

Cross-Silo Federated Learning for Multi-Tier Networks with Vertical and Horizontal Data Partitioning

ANIRBAN DAS, Rensselaer Polytechnic Institute, USA

SHIQIANG WANG, IBM Research, USA

STACY PATTERSON, Rensselaer Polytechnic Institute, USA

We consider federated learning in tiered communication networks. Our network model consists of a set of silos, each holding a vertical partition of the data. Each silo contains a hub and a set of clients, with the silo's vertical data shard partitioned horizontally across its clients. We propose Tiered Decentralized Coordinate Descent (TDCD), a communication-efficient decentralized training algorithm for such two-tiered networks. To reduce communication overhead, the clients in each silo perform multiple local gradient steps before sharing updates with their hub. Each hub adjusts its coordinates by averaging its workers' updates, and then hubs exchange intermediate updates with one another. We present a theoretical analysis of our algorithm and show the dependence of the convergence rate on the number of vertical partitions, the number of local updates, and the number of clients in each hub. We further validate our approach empirically via simulation-based experiments using a variety of datasets and objectives.

CCS Concepts: • **Computing methodologies** → **Machine learning algorithms**; **Distributed algorithms**; **Neural networks**; • **Mathematics of computing** → **Nonconvex optimization**.

Additional Key Words and Phrases: coordinate descent, federated learning, machine learning, stochastic gradient descent

1 INTRODUCTION

In recent times, we have seen an exponential increase in the amount of data produced at the edge of communication networks. In many settings, it is infeasible to transfer an entire dataset to a centralized cloud for downstream analysis, either due to practical constraints such as high communication cost or latency, or to maintain user privacy and security [10]. This has led to the deployment of distributed machine learning and deep-learning techniques where computation is performed collaboratively by a set of clients, each close to its own data source. Federated learning has emerged as a popular technique in this space, which performs iterative collaborative training of a global machine learning model over data distributed over a large number of clients, without sending raw data over the network.

The more commonly studied approach of federated learning is *horizontal federated learning*. In horizontal federated learning, the clients' datasets share the same set of features, but each client holds only a subset of the sample space, i.e., the data is horizontally partitioned among clients [10, 13, 18]. In this setting, the clients train a copy of a model on their local datasets for a few iterations and then communicate their updates in the form of model weights or gradients directly to a centralized parameter server. The parameter server then creates the centralized model by aggregating the individual client updates and the process is repeated until a desired convergence criterion is met.

Another scenario that arises in federated learning is when clients have different sets of features, but there is a sizable overlap in the sample ID space among their datasets [27]. For example, the training dataset may be distributed across silos in a multi-organizational context, such as in healthcare, banking, finance, retail, etc. [21, 27]. Each silo holds a distinct set of features (e.g., customer/patient list); the data within each silo may even be of a different modality, for example,

one silo may have audio features, whereas another silo has image data. Further, the silos may not want to share data with the other silos directly. The paradigm of training a global model over such feature-partitioned data is called *vertical federated learning* [16, 28].

A common approach for model training over vertically partitioned data builds on parallel coordinate gradient descent-type algorithms [11, 17, 19]. Here, silos execute independent training iterations in parallel to each optimize a global model along its subset of coordinates. The silos exchange intermediate information to ensure that the parallel updates lead to convergence of the global model. In early vertical federated learning works [3, 5, 28], the silos exchange intermediate information after every local training iteration. However, such frequent information exchanges can lead to high training latency, especially when the communication latency is high and the intermediate information is large. A more recent work [16] proposed an algorithm that addresses the problem by performing multiple local training iterations in each silo before the silos exchange intermediate information for the next round of training. All of these works assume that the entire dataset owned by a silo is contained in a single client.

However, in silos with a large organizational structure, it is natural that the data will be distributed across multiple clients. Previous works fail to capture the case where the dataset within each silo is further horizontally partitioned across multiple clients. As a motivating example, we consider two smartphone application providers who wish to train a global model over the datasets stored on the smartphones of their respective customer bases. Here, the two application companies do not want to share the customer data directly with each other. At the same time, the users do not want to share raw personal data with the companies. In this case, the data is vertically partitioned across different the applications of the different companies. Further, the data of a single company is horizontally partitioned across different application users. The silos can be thought of as the top *tier* of our system architecture. The clients inside the silos can be thought of as the bottom *tier*.

We can think of another use case when there is a large overlap in the customer ID space between a banking silo \mathcal{B} , e.g, a banking holding company with multiple independent subsidiary banks, and an insurance silo \mathcal{I} , e.g., an insurance holding company with multiple independent subsidiaries. The two silos want to build a global model collaboratively to predict credit score, for example. Here, the entire data is vertically partitioned between the bank and the insurance holding companies in the top tier. Each subsidiary of \mathcal{B} acts as a client and may have a separate customer base, operating in a separate geographical location in a country. Thus the entire customer data of the bank silo is horizontally partitioned across its subsidiaries in the bottom tier. Silo \mathcal{I} for the insurance holding company also has a similar structure. Silos \mathcal{B} and \mathcal{I} do not want to share information directly with each other. Further, each subsidiary within a silo may not be able to frequently share huge amounts of raw information with all other subsidiaries within the same silo, due to either policy, privacy/security concerns, regulations, or even bandwidth limitations in the communication network. Training a global model in presence of both vertical and horizontal partitioning of data in a communication efficient manner and analyzing its convergence is not straightforward. The vertical partitioning of data makes the setting different from simple horizontal federated learning. Also, since each client in a silo will update its own set of coordinates in parallel with other clients, this setting is also different from earlier vertical federated learning works with a single tier.

We propose Tiered Decentralized Coordinate Descent (TDCD), a federated learning algorithm for training over data that is vertically partitioned across silos and further horizontally partitioned within silos. Each silo internally consists of multiple clients connected to a hub, which is a server in the silo. The hub can be a cloud server maintained by the mobile application company. The hub can also be a server maintained by the company in charge of orchestrating the IT infrastructure of a particular silo. A hub itself does not contain data but facilitates training by coordinating information. The goal is to jointly train a model on the features of the data contained across silos,

without explicitly sharing raw data between the clients and the hubs, and between clients across different silos.

TDCD works by performing a non-trivial combination of parallel coordinate descent on the top tier between silos and distributed stochastic gradient descent with multiple local steps per communication round in the bottom tier of clients inside each silo. More specifically, each hub maintains a block of the trainable parameters. Clients within a silo train these parameters on their local data sets for multiple iterations. The hub then aggregates the client models to update its parameter block. To execute the local iterations, clients need some form of embeddings from the data from clients in other silos. The hubs orchestrate this information exchange every time they update their parameter blocks. By waiting for several training iterations to exchange this information, this helps reduce the communication cost of the algorithm. Our approach is thus a novel communication efficient combination of learning with both vertically and horizontally partitioned data in a multi-tiered network.

Specifically, our contributions are the following:

- (1) We present a system model for decentralized learning in a two-tier network, where data is both vertically and horizontally partitioned.
- (2) We develop a communication-efficient decentralized learning algorithm using principles from coordinated descent and stochastic gradient descent.
- (3) We analyze the convergence of our proposed algorithm for non-convex objectives and show how it depends on the number of silos, the number of clients, and the number of local training steps. With appropriate assumptions, we achieve a convergence rate of $O\left(\frac{1}{\sqrt{T}}\right)$.
- (4) We validate our analysis via experiments using different objectives and different datasets. We further explore the effect of communication latency on the convergence rate.

We observe from our experiments that, when communication latency is large with respect to the computation latency at the clients, a larger number of local iterations leads to faster convergence. However, if the number of local iterations Q is too large then for the selected learning rate, the algorithm may diverge. Further, our experimental observation suggests that TDCD shows little performance degradation as the number of vertical and horizontal partitions increases.

1.1 Related Work

Iterative training of machine learning models with vertically-partitioned features has been studied in the context of coordinate descent algorithms. A coordinate descent algorithm with gradient steps was first proposed in [22], where a fully centralized system is considered. In a decentralized context, parallel coordinate descent methods have been proposed in [11, 17, 19]. These algorithms typically require a shared memory architecture or raw data sharing and shuffling of the vertical partitions between the workers. Since TDCD operates in a federated learning setting, such access to raw data and shared memory is not possible, and therefore, these algorithms are not applicable.

In recent years, in distributed learning where data is horizontally partitioned across multiple clients, periodic averaging based methods like federated averaging and its variations have been extensively studied. Federated averaging type methods have been studied in the context of convex objectives [12, 20, 26] and non-convex objectives [6, 15, 23, 29] in presence of either IID or non-IID distribution of data. The common approach is to take multiple (stochastic) gradient steps in parallel locally to achieve better communication efficiency as well preserve privacy by not sharing the raw data. Other works have analyzed versions of horizontal federated learning for hierarchical or multi-tier networks, where data is partitioned horizontally across all clients participating in the process [2, 24, 25].

In the context of distributed training with vertical partitions in a federated setting, [7] proposed a system with two silos communicating via a third-party coordinating service. Extending on this, [28] removed the need of the third party coordinator but focused on the communication patterns of logistic regression. The algorithms in these earlier works are specific for two vertical partitions and do not exploit multiple local training iterations. The authors in [5] model the vertical federated learning problem as an alternating optimization problem, but their system model consists of a single tier and the focus is mainly on estimating the labels independently at each worker device using a collaborative approach. The work [3] proposed an asynchronous vertical federated learning approach in a single tier network. Such earlier works only considered the case when each party communicates in each iteration of training, which is communication-wise expensive. A more recent work on vertical federated learning [16] solves this problem by allowing clients to take multiple local steps of training before communicating to the hub. However, all these works only address the case where all data in a silo is contained within a single client. In this work, we consider vertical and horizontal partitions of the dataset simultaneously in the two tiers: silos and clients inside silos. TDCD thus performs model training in such a multi-tiered system architecture by fusing horizontal and vertical learning approaches in a novel manner.

1.2 Paper Outline

The rest of the paper is organized as follows. We describe our system model, data partitioning, and loss function in Section 2. In Section 3, we present TDCD, followed by its convergence analysis in Section 4. The proof of the theorem and supporting lemmas are deferred to Appendix A. We provide experimental evaluation of TDCD in Section 5 and finally conclude in Section 6.

2 SYSTEM MODEL AND PROBLEM FORMULATION

In this section, we describe the system architecture, the allocation of the training data, and the loss function we seek to minimize.

2.1 System Architecture and Training Data

We consider a decentralized system consisting of N silos, shown Fig. 1a. Each silo consists of a hub and multiple clients connected to it in a hub-and-spoke fashion. Each silo j has K_j clients. The number of clients per silo may be unequal. Our network model thus has two tiers: the top tier of hubs, shown in orange, that communicate with each other, and the bottom tier of clients in each silo, shown in gray. If we map this system model on the bank and insurance example in Section 1, there would be two silos, a banking silo corresponding to a banking holding company and an insurance silo corresponding to an insurance holding company. The clients in the banking silo could be subsidiary banks of the banking holding company, and similarly, for the insurance silo, the clients could be different divisions of the insurance holding company.

The training data consists of M sample IDs that are common across all silos. This means that across all N silos, there are M sample IDs that are common. Each sample has D features. The data is partitioned vertically across the N silos so that each silo owns a disjoint set of D_j features for all of the M sample IDs. More formally, we can express the entire training dataset by a matrix $\mathbf{X} \in \mathbb{R}^{M \times D}$. We denote the set of data, i.e., the columns of \mathbf{X} , held in silo j by \mathbf{X}_j . The vertical slice of data in silo j , \mathbf{X}_j , is, therefore, a matrix of dimension $M \times D_j$. Within each silo, its data is partitioned horizontally across its clients, so that each client holds some rows of \mathbf{X}_j . We denote the horizontal shard of \mathbf{X}_j that is held by client k in silo j as the matrix $\mathbf{X}_{k,j}$. Lastly, we denote a sample p of the dataset (single row of \mathbf{X}) as $\mathbf{X}^{(p)}$, and $\mathbf{X}_j^{(p)}$ denotes the features of the p th sample corresponding to silo j . We note that the features corresponding to a sample ID p , $\mathbf{X}_{k,j}^{(p)}$ will only be present in

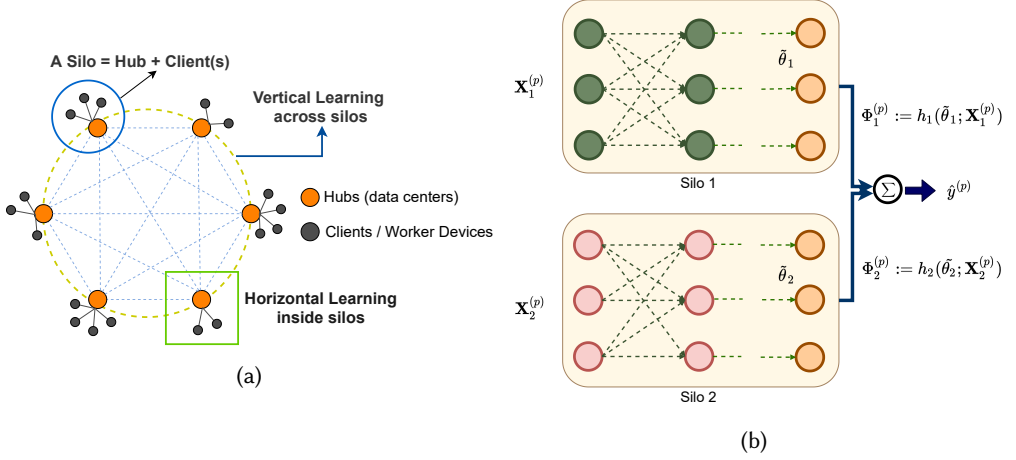


Fig. 1. System Model: (a) System architecture., (b) Example clients models and the input and output to the system. Figure shows a client k at each of the two silos and the concatenation of their output embedding to find the target \tilde{y} corresponding to a single data sample p .

any one client k among all the clients in the silo j . To simplify notation, we will therefore use $\mathbf{X}_j^{(p)}$ instead of $\mathbf{X}_{k,j}^{(p)}$ to denote the features for sample ID p contained in silo j in the rest of the paper. A sample ID in the banking and insurance example would correspond to an individual who is a common customer to both the banking and the insurance silos. The features of samples in the banking clients would consist of features such as balance, installments, debit history, credit history, etc. Similarly, the data in the clients of the insurance organization would have insurance related features such as policy details, premium, age, dependent information, past claims, etc.

We assume that each client stores the sample labels $\mathbf{y}_{k,j}$ for its data $\mathbf{X}_{k,j}$. For the same sample ID, the labels stored across the silos are the same. In many low-risk scenarios, such as credit history, labels can be shared across silos. Labels can also be shared when the sample IDs themselves are anonymized. In scenarios where the labels are sensitive, for example, the case when the labels are only present in a single silo, it is still possible to extend TDCD to without label sharing, albeit with extra communication steps, in an approach similar to [16]. We elaborate on this further in Section 3, Remark 2.

2.2 Model Formulation and Loss Function

The objective is to train a global model $\tilde{\theta}$, that can be decomposed into N coordinate block partitions, each corresponding to the model parameters assigned to a silo:

$$\tilde{\theta} = [\tilde{\theta}_1^\top, \dots, \tilde{\theta}_N^\top]^\top \quad (1)$$

where each $\tilde{\theta}_j$ is the block of coordinate partition for silo j . $\tilde{\theta}$ could be weights of a linear model such as linear or logistic regression, for example, or could be trainable weights of a neural network. Let us represent the function computed by a silo j as h_j , where h_j is a map from the higher dimensional input space \mathbf{X}_j to the lower dimensional embedding space Φ_j parameterized by $\tilde{\theta}_j$. We denote the embedding learned by silo j for a sample p with $\Phi_j^{(p)} \stackrel{\text{def}}{=} h_j(\tilde{\theta}_j; \mathbf{X}_j^{(p)})$.

We denote the loss corresponding to a data sample p with features $\mathbf{X}^{(p)}$ with its label $y^{(p)}$ by $\ell(\Phi_1^{(p)}; \Phi_2^{(p)}; \dots; \Phi_N^{(p)}; y^{(p)})$. The goal of the training algorithm is to minimize an objective function

with following structure:

$$\min_{\tilde{\theta}} \mathcal{L}(\tilde{\theta}; \mathbf{X}; \mathbf{y}) \stackrel{\text{def}}{=} \frac{1}{M} \sum_{p=1}^M \ell(\Phi_1^{(p)}; \Phi_2^{(p)}; \dots; \Phi_N^{(p)}; y^{(p)}). \quad (2)$$

where $\Phi_j^{(p)} = h_j(\tilde{\theta}_j; \mathbf{X}_j^{(p)})$. Further, the function ℓ has the following separable form:

$$\ell(\Phi_1^{(p)}; \Phi_2^{(p)}; \dots; \Phi_N^{(p)}; y^{(p)}) \stackrel{\text{def}}{=} f\left(\sum_{j=1}^N h_j(\tilde{\theta}_j; \mathbf{X}_j^{(p)}); y^{(p)}\right). \quad (3)$$

Our objective function \mathcal{L} can be non-convex. Since ℓ is a function of $\tilde{\theta}$, consequently, \mathcal{L} is clearly a function of $\tilde{\theta}$. The trainable parameters here are $\tilde{\theta}_j$, $j = 1, \dots, N$. When the context is clear, we drop \mathbf{X}, \mathbf{y} from $\mathcal{L}(\cdot)$ for simplifying notation.

In Fig. 1b we show the logical view of our global model in Equation 1, mapped onto our physical system architecture. In this concrete example, the global model is a neural network partitioned across silos. Each silo maintains a logical partition of the overall neural network model, where each partition is also a neural network of one or multiple layers. The weights are trained by the individual silos. Further, each silo, as mentioned in Section 2.1, is assigned a vertical slice of the entire set of data. For example, in Fig. 1b, we have two silos, Silo 1 and Silo 2. The neural network models in each silo can be thought of as embedding generating functions that feed in corresponding input feature partitions of data present in the silo and generate embeddings for sample IDs in the data. This overall effect of such an architecture is that the penultimate trainable layer of the models of all the silos are effectively concatenated as a linear layer. The output of the concatenated linear layer is fed into the classifier/regressor node for generating target values.

In a physical system, we realize this logical architecture as follows: each client in a silo j holds a copy of the neural network architecture represented by h_j . Each client can then independently compute embedding $\Phi_j^{(p)}$ if p is a sample ID contained in that client. For the rest of the paper, we use the neural network model described above as our reference architecture. Of note, since the hubs are all connected to one another, they can exchange the embeddings $\Phi_j^{(p)}$ with each other.

3 PROPOSED ALGORITHM

In this section, we present our Tiered Decentralized Coordinate Descent algorithm. The pseudocode is given in Algorithm 1.

We first note that the hubs update their own corresponding blocks of coordinates of $\tilde{\theta}_j$ in parallel; no hub stores the entire model $\tilde{\theta}$. We define $\theta_{k,j}^t$ as the local version of the coordinates of the weight vector $\tilde{\theta}_j^t$ that each client updates. These local versions are initialized by the clients at iteration $t = 0$.

In Algorithm 1, in iteration $t = 0$, and every Q th iteration thereafter, the hubs first average the models from the clients, where hub j updates the j th block coordinates of global weight vector $\tilde{\theta}^t$ as $\tilde{\theta}_j^t = \frac{1}{K_j} \sum_{k=1}^{K_j} [\theta_{k,j}^t]$. This step is similar to horizontal federated learning. The hubs then select a single minibatch ζ , containing B samples randomly drawn from the global dataset \mathbf{X} .¹ The hubs communicate the aggregated model and information regarding the sample IDs chosen in the minibatch to their clients. The clients, in turn, reply with the intermediate information for the samples IDs in that minibatch using the newest aggregated model.

¹This can be achieved for example via pseudo random number generators across silos initialized with the same seed.

Algorithm 1 Tiered Decentralized Coordinate Descent (TDCD)

```

1: Initialize  $\theta_{k,j}^t = \theta_{k,j}^{init}, \forall k, j$ 
2: for  $t \leftarrow 0, \dots, T$  do
3:   if  $t \pmod{Q} = 0$  then
4:     Randomly sample a minibatch  $\zeta^{t_0}$ .
5:     for  $j \leftarrow 1, \dots, N$  silos in parallel do
6:       Hub  $j$  computes  $\tilde{\theta}_j^t \leftarrow \frac{1}{K} \sum_{k=1}^K \theta_{k,j}^t$ 
7:       for  $k \leftarrow 1, \dots, K_j$  clients in parallel do
8:         Set  $\theta_{k,j}^t \leftarrow \tilde{\theta}_j^t$ 
9:         Send  $\Phi_{k,j}^{\zeta^{t_0}}$  to hub  $j$ 
10:      end for
11:    end for
12:    for  $j \leftarrow 1, \dots, N$  silos in parallel do
13:      Hub  $j$  stacks  $\{\Phi_{k,j}^{\zeta^{t_0}}\} \forall k$  to obtain  $\Phi_j^{\zeta^{t_0}}$ 
14:      All hubs exchange  $\Phi_j^{\zeta^{t_0}}, j = 1, \dots, N$ 
15:      Hub  $j$  calculate  $\Phi_{-j}^{\zeta^{t_0}} \leftarrow \sum_{l=1, l \neq j}^N \Phi_l^{\zeta^{t_0}}$ 
16:      for  $k \leftarrow 1, \dots, K_j$  clients in parallel do
17:        Set  $\Phi_{-k,j}^{\zeta^{t_0}} \leftarrow \pi_{k,j}(\Phi_{-j}^{\zeta^{t_0}})$ .
18:      end for
19:    end for
20:  end if
21:  for  $j \leftarrow 1, \dots, N$  silos in parallel do
22:    for  $k \leftarrow 1, \dots, K_j$  clients in parallel do
23:       $\theta_{k,j}^{t+1} \leftarrow \theta_{k,j}^t - \eta g_{k,j}(\Phi_{-k,j}^{\zeta^{t_0}}, \Phi_{k,j}^{\zeta^{t_0}}; \zeta^{t_0})$ 
24:    end for
25:  end for
26: end for

```

Next, the system computes the information needed for each client to calculate its local stochastic partial derivatives. We call the embedding $\Phi_j^{(p)}$ the *intermediate information* for the j th coordinate block for a single sample p .² For hub j , we denote the intermediate information obtained from other hubs by $\Phi_{-j}^{(p)} \stackrel{\text{def}}{=} \sum_{l=1, l \neq j}^N \Phi_l^{(p)}$. Let Φ_{-j}^{ζ} denote the entire intermediate information of silos other than silo j , that is received by silo j for minibatch ζ . We similarly denote $\Phi_{k,j}^{\zeta}$ and $\Phi_{-k,j}^{\zeta}$ as the information from Φ_j^{ζ} and Φ_{-j}^{ζ} from a minibatch ζ held by client k of silo j . Now, let $g_{k,j}$ denote the local stochastic partial derivative of the loss function with respect to the block of coordinates j in client k . The vector $g_{k,j}$ is a function of the intermediate information from all the silos, and is defined as the following:

$$g_{k,j}(\Phi_{-k,j}^{\zeta}, \Phi_{k,j}^{\zeta}; \zeta) \stackrel{\text{def}}{=} \frac{1}{|\zeta|} \sum_{p \in \zeta} \nabla_{\theta_{k,j}} \ell(\Phi_1^{(p)}; \Phi_2^{(p)}; \dots; \Phi_N^{(p)}; y^{(p)}). \quad (4)$$

²We use embedding and intermediate information interchangeably in this paper.

In TDCD, to obtain the set of intermediate information for a single minibatch ζ , a client k in a silo j then computes the set of information $\Phi_{k,j}^\zeta = \{\Phi_j^{(p)}\}_{p \in \zeta}$ via a forward propagation through its local neural network and sends it to its hub. Each hub then stacks the set of updates $\{\Phi_{k,j}^\zeta\}$ from each of its clients to obtain Φ_j^ζ , which can be then used to find the empirical loss for the batch of minibatch samples. Each hub j for silo j broadcasts Φ_j^ζ to all of the other hubs to propagate this information. Following these broadcasts, each hub j has the intermediate information of other hubs Φ_{-j}^ζ . We define a projection function $\pi_{k,j}$ such that $\pi_{k,j}(\Phi_{-j}^\zeta) = \Phi_{-k,j}^\zeta$, where $\Phi_{-k,j}^\zeta$ is the information from Φ_{-j}^ζ that is relevant to samples held by k of silo j . The hub then sends $\Phi_{-k,j}^\zeta$ to each of its clients k . Alternatively, a hub can send the entire Φ_{-j}^ζ to the client and the client can extract the rows corresponding to its own samples. After receiving this intermediate information, each client k of silo j can now calculate its own local stochastic partial derivative.

Each client in TDCD then executes Q local stochastic gradient steps on the feature block of its silo using the same minibatch for the Q consecutive iterations:

$$\theta_{k,j}^{t+1} = \theta_{k,j}^t - \eta g_{k,j}(\Phi_{-k,j}^{\zeta^{t_0}}, \Phi_{k,j}^{\zeta^{t_0}}; \zeta^{t_0}). \quad (5)$$

Here η is the step size (learning rate), and t_0 represents the most recent iteration $t_0 < t$ in which the client received intermediate information from the other silos. Thus, when a client executes multiple local gradient steps to update $\theta_{k,j}^t$, it recalculates its local embedding $\Phi_{k,j}^{\zeta^{t_0}}$. However, it uses the identical intermediate information $\Phi_{-k,j}^{\zeta^{t_0}}$ from other silos throughout the Q iterations of local training. Therefore the information after iteration $t_0 + 1$ is effectively stale. The entire process from start to the completion of Q iterations of parallel training inside silos comprises a *global round* or a *communication round*, and this global round is repeated until convergence.

In TDCD, clients only communicate their local model and intermediate information every Q iterations. This is in contrast to distributed SGD algorithms, where the clients need to synchronize with a coordinating hub in each iteration. This allows TDCD to save bandwidth by increasing Q , especially when the size of the model is large. The significant bandwidth savings come in the silos themselves, since each hub and its clients only share the models and intermediate information for a single minibatch every Q iterations. As a rough estimate, the intermediate information for a sample ranges from a simple scalar value to a small vector of very few dimensions. Therefore while training models in deep learning, the intermediate information of B minibatches with M samples each would be in the order of a few megabytes or less. Compared to this, the size of the actual model can be in the order of gigabytes. We explore how Q impacts the convergence of TDCD in the next section.

Remark 1. We note that the hubs form a fully connected graph. Each hub maintains a non-overlapping block of parameters of the full global model. At the end of the training process (or at some intermediate time) the hubs can share their parameter blocks with one another so that each silo has the full global model for inference purposes.

Remark 2. We assume that every client has the labels for all of its samples. However, in cases when the labels are sensitive and sharing the labels for a sample ID across silos is not feasible, the label information for a sample ID may only be present in a client in one silo. In this case, we could modify our algorithm in the following way, similar to [16]: the clients in all silos send the intermediate information for a sample to the client that has the label for the sample. The client with the label information calculates the loss and the partial derivatives which can then be propagated back to

the other clients for use in the local gradient steps. This modification would greatly increase the communication cost of the algorithm. We note that the modified algorithm would be mathematically equivalent to TDCD albeit with higher communication cost, and hence the convergence analysis given in Section 4 can be trivially extended to that case.

4 CONVERGENCE ANALYSIS

In this section, we provide the convergence analysis of the TDCD algorithm. We first make the following set of common assumptions [1, 16, 29] about the loss function \mathcal{L} and the local partial derivatives $g_{k,j}$ at each client.

ASSUMPTION 1. *The gradient of the loss function is Lipschitz continuous with constant L ; further, the partial derivative of \mathcal{L} , with respect to each coordinate block j , denoted by $\nabla_{(j)}\mathcal{L}(\cdot)$, is Lipschitz continuous with constant L_j , i.e., for all $\theta_1, \theta_2 \in \mathbb{R}^D$*

$$\|\nabla\mathcal{L}(\theta_1) - \nabla\mathcal{L}(\theta_2)\| \leq L \|\theta_1 - \theta_2\| \quad (6)$$

$$\|\nabla_{(j)}\mathcal{L}(\theta_1) - \nabla_{(j)}\mathcal{L}(\theta_2)\| \leq L_j \|\theta_1 - \theta_2\|. \quad (7)$$

ASSUMPTION 2. *The function \mathcal{L} is lower bounded so that for all $\theta \in \mathbb{R}^D$, $\mathcal{L}(\theta) \geq \mathcal{L}_{\inf}$.*

ASSUMPTION 3. *Let ζ be a mini-batch drawn uniformly at random from all samples. Then, for all $\theta \in \mathbb{R}^D$,*

$$\mathbb{E}_{\zeta} \left[g_{k,j}(\Phi_{-j}^{\zeta}, \Phi_j^{\zeta}; \zeta) \right] = \nabla_{(j)}\mathcal{L}(\theta) \quad (8)$$

$$\mathbb{E}_{\zeta} \left[\|g_{k,j}(\Phi_{-j}^{\zeta}, \Phi_j^{\zeta}; \zeta) - \nabla_{(j)}\mathcal{L}(\theta)\|^2 \right] \leq \sigma_j^2. \quad (9)$$

where the expectation is over the choice of minibatch ζ . Recall $\Phi_j^{\zeta} = h_j(\theta; \mathbf{X}_j^{\zeta})$ for a given θ and hence the partial derivatives $g_{k,j}$ are functions of θ .

We also use the following definition:

$$L_{\max} \stackrel{\text{def}}{=} \max_{1 \leq j \leq N} L_j.$$

Our analysis is based on the evolution of the global model $\tilde{\theta}$ following Algorithm 1. It is noted that the components of $\tilde{\theta}$, $\tilde{\theta}_j$ are realized every Q iterations, but for theoretical analysis we study the evolution of a virtual $\tilde{\theta}_j$ at each iteration with $\tilde{\theta}_j^t = \frac{1}{K} \sum_{k=1}^K \theta_{k,j}^t$.

We further define the following two quantities :

$$\mathbf{G}_{(j)}^t = \frac{1}{K_j} \sum_{k=1}^{K_j} g_{k,j}(\Phi_{-k,j}^{\zeta^t}, \Phi_{k,j}^{\zeta^t}; \zeta^t) \quad (10)$$

$$\mathbf{G}^t = [(\mathbf{G}_{(1)}^t)^T, \dots, (\mathbf{G}_{(N)}^t)^T]^T. \quad (11)$$

We can then write the evolution of the global model as follows,

$$\tilde{\theta}^{t+1} = \tilde{\theta}^t - \eta \mathbf{G}^t. \quad (12)$$

We now provide the main theoretical result of this paper. The proof is deferred to the appendix.

THEOREM 1. *Under Assumptions 1, 2, and 3, when the step size η satisfies the following condition:*

$$0 \leq \eta \leq \min \left(\frac{1}{L}, \frac{1}{L_{\max} Q \sqrt{N}} \right) \quad (13)$$

then, for $T > 0$, the expected squared norm of the gradient of \mathcal{L} , averaged over $T > 0$ iterations, satisfies the following bound:

$$\mathbb{E} \left[\frac{1}{T} \sum_{t=0}^{T-1} \|\nabla \mathcal{L}(\tilde{\theta}^t)\|^2 \right] \leq \frac{2}{\eta T} \left(\mathcal{L}(\tilde{\theta}^0) - \mathcal{L}_{inf} \right) + \eta L \sum_{j=1}^N \frac{\sigma_j^2}{K_j} + L_{max}^2 \eta^2 Q^2 N \sum_{j=1}^N \sigma_j^2. \quad (14)$$

The convergence error in Theorem 1 results from the parallel updates on the coordinate blocks which depends on the number of vertical partitions N , staleness due to multiple local iterations, i.e., the value of Q , and due to parallel updates based on horizontal partitioning across K_j clients in silo j . With an increase in the number of vertical partitions N , the error term increases linearly. The error also depends quadratically on Q ; however, in practice, if Q is offset by a suitable learning rate η , then we can leverage multiple local iterations to achieve faster convergence in terms of wall clock time, as we show in Section 5. Choosing a very small η will decrease the convergence error, but it will but increase the first term on the right hand side of (14), leading to slower convergence.

Remark 3. When $N = 1$, i.e., there is only one silo, then the algorithm reduces to local SGD with horizontally partitioned data partitioning, and the convergence rate is similar to that obtained in [29] with respect to the order of Q, K_j, L .

Remark 4. When $K_j = 1$, for $j = 1, 2, \dots, N$, i.e., there exists only one client per silo, the algorithm reduces to vertical federated learning with a single tier, and the convergence rate is similar with respect to the orders of Q, N, L to that obtained in [16].

Remark 5. If we select $\eta \propto \frac{1}{\sqrt{T}}$ and $Q \propto T^{\frac{1}{4}}$, then the (average) expected gradient norm squared converges with a rate of $\mathcal{O}\left(\frac{1}{\sqrt{T}}\right)$, similar to [16].

5 EXPERIMENTAL RESULTS

We verify the convergence properties of TDCD with respect to the different algorithm parameters of the system via a simulation. For simplicity, in our experiments, each client in a silo has the same number of samples $\frac{M}{K_j}$, $j = 1, 2, \dots, N$.

5.1 Datasets and Models

We first briefly discuss the two datasets used in this study.

Cifar10: We train a CNN model on the Cifar10 dataset [14]. Cifar10 is a set of $3 \times 32 \times 32$ pixels color images with 50,000 images in the training set and 10,000 images in the test. We use $N = 2$ for all the experiments and divide each Cifar10 image vertically into two parts in all three channels ($3 \times 32 \times 16$). Each silo trains a local CNN model with a shared linear classifier layer at the top that uses cross-entropy loss. We assign the left ($3 \times 32 \times 16$) vertical partition of all images in one silo and the right vertical partition of all images in the other silo. The local CNNs have two convolutional layers, three fully connected layers. The output embeddings of the last layer is of dimension \mathbb{R}^{10} and can be fed into a cross entropy function along with outputs from other silos to generate the target. We thus train the parameters of the local CNN model via TDCD.

MIMIC-III: We train an LSTM model using the MIMIC-III (Medical Information Mart for Intensive Care) [9] dataset, which consists of anonymized information of patients admitted to critical care units in a hospital. We follow the data processing steps from [8] to obtain 14,681 training samples and 3,236 test samples. Each sample consist of 48 time steps corresponding to 48 hours, and each time step is of 76 features. For training we split the data vertically along the feature axis. The goal is to predict in-hospital-mortality rate as a binary classification task. Each silo trains an

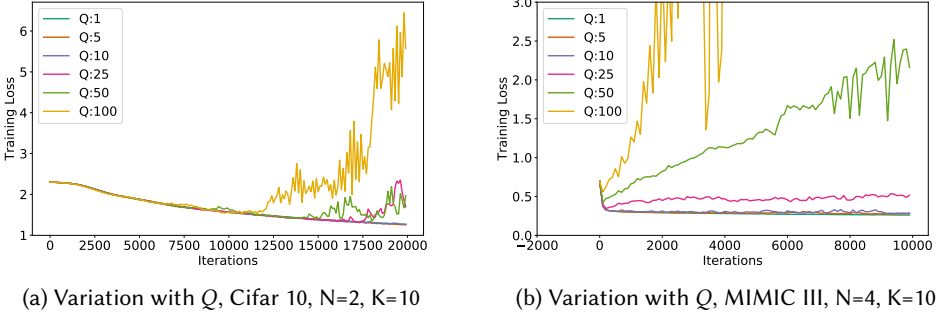


Fig. 2. Performance of a CNN on Cifar10 dataset and LSTM on MIMIC III, training loss vs iterations t for various values of Q i.e., the number of local iterations.

LSTM model consisting of two LSTM layers, and a linear layer on the top, with binary cross entropy as class prediction output. We train the parameters of the local LSTM model via TDCD.

5.2 Experimental Setup

In all figures, N represents the number of silos (vertical partitions of the dataset), and K represents the number of clients in each silo. In each of the experiments, the training loss is calculated using the global model $\tilde{\theta}$ and the full training data matrix at some multiples of Q iterations. Each Q th iteration is a *communication round* because that is when communication between clients and hubs, and between hubs occurs. Across all experiments, we use a minibatch size of 1250 unless otherwise specified.³ Across all experiments, unless otherwise specified, we use fixed learning rate $\eta = 0.002$ for the experiments with Cifar10 and $\eta = 0.0005$ for the experiments with MIMICIII.

We further note that the convergence of TDCD with respect to the training loss on training dataset is shown in this section. The raw performance on the unseen test dataset is provided in Appendix B for all the experiments.

5.3 Results

Here we describe our experimental results.

5.3.1 Effect of Q . We study the convergence of TDCD with various numbers of local training iterations Q . The results are shown in Fig. 2a and Fig. 2b. In both the figures in this experiment, on the X-axis we have training iterations and on the Y-axis we plot training loss. In Fig. 2a, we fix the number of vertical partitions to $N = 2$ and horizontal partitions to $K = 10$. In Fig. 2b, we fix the number of vertical partitions to $N = 4$ and horizontal partitions to $K = 10$. In both experiments, we vary the number of local iterations Q between 1 to 100. In both cases, we observe that with increasing Q , the convergence rate actually worsens in terms of iterations. If the number of local iterations Q is too large for the selected learning rate, the algorithm may diverge. Further, prolonged local training without reconciling with the global models tends to slow training and adds to the convergence error. Theorem 1 gives conditions on the learning rate to guarantee convergence and the dependence of convergence error on Q . However, we shall see later in Section 5.3.4 that higher

³This batch size is the total batch size across all horizontal partitions in the silo at an iteration. Hence each client ends up with a fraction of samples from the 1250 sized batch. For example, in a silo which has 10 clients, if the batch size is 1250, each of the 10 clients will in expectation have training batch size of 125 at every training iteration.

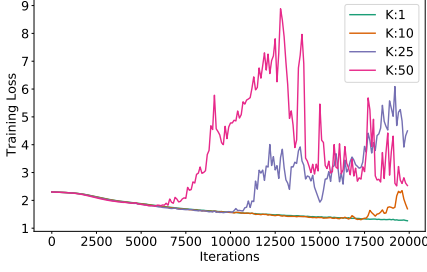
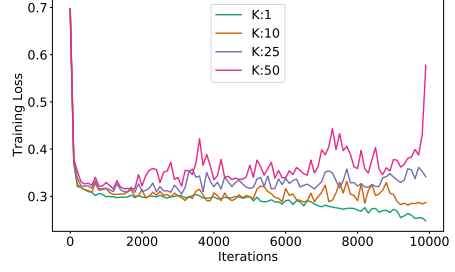
(a) Variation with K , Cifar 10, $N=2$, $Q=25$ (b) Variation with K , MIMIC III, $N=4$, $Q=10$

Fig. 3. Performance of a CNN on Cifar10 dataset and LSTM on MIMIC III, training loss vs iterations t for various values of K i.e., the number of horizontal partitions.

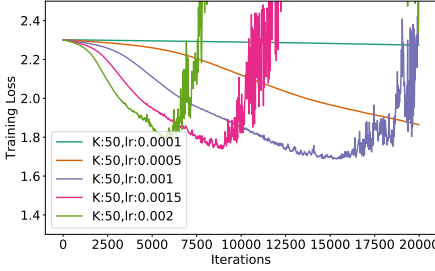
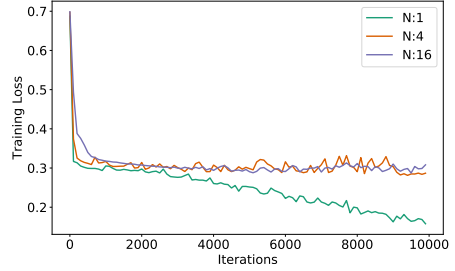
(a) Variation of η with high K , Cifar 10, $N=2$, $Q=25$ (b) Variation with N , MIMIC III, $K=10$, $Q=10$

Fig. 4. (a) Performance of a CNN on Cifar10 dataset effect of η on large values of K (b) Performance of LSTM on MIMIC III, training loss vs iterations t for various values of N i.e., number of vertical partitions.

values of Q achieve faster convergence when we consider training latency instead of training iterations.

5.3.2 Effect of number of horizontal partitions K . For the next experiment, we study the effect of the number of horizontal partitions by varying K . For Cifar10 in Fig. 3a, we fix $N = 2$ and $Q = 25$, and for MIMIC III in Fig. 3b, we fix $N = 4$ and $Q = 10$. The values of Q are selected based on the previous experiment. It is to be noted that we are studying the case when the entire vertically-partitioned dataset is divided horizontally among the K clients in each silo. This means that with higher values of K , each client will hold fewer samples. We observe that convergence rate is worse with higher values of K . This can be attributed to the increase in the variance of the trained models. For example, in Fig. 3a, the cases with $K = 25$ and $K = 50$ diverge. However, by reducing the learning rate appropriately, even large values of K can be made to converge. In Fig. 4a, we again consider $K = 50$ and plot the convergence rate for different learning rates. We observe that TDCD still converges for learning rates < 0.001 . For a fixed learning rate, having a lower number of horizontal partitions is observed to be beneficial for faster convergence.

5.3.3 Effect of number of vertical partitions N . We now study the effect of number of the number vertical partitions N . We show the results in Fig. 4b for the MIMIC III dataset. We pick $Q = 10$ and $K = 10$ and keep them constant throughout this set of experiments. We observe that the convergence is worse for higher values of N for the same learning rate. This is expected from

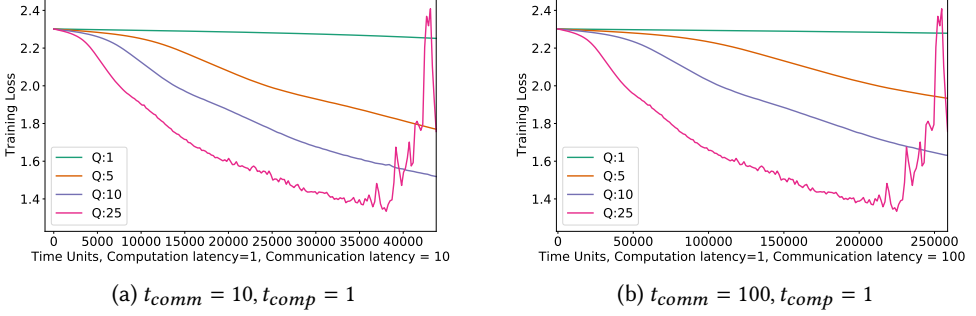


Fig. 5. CNN on CIFAR 10, training loss vs time units for variations of t_{comm} . $N=2, K=10$.

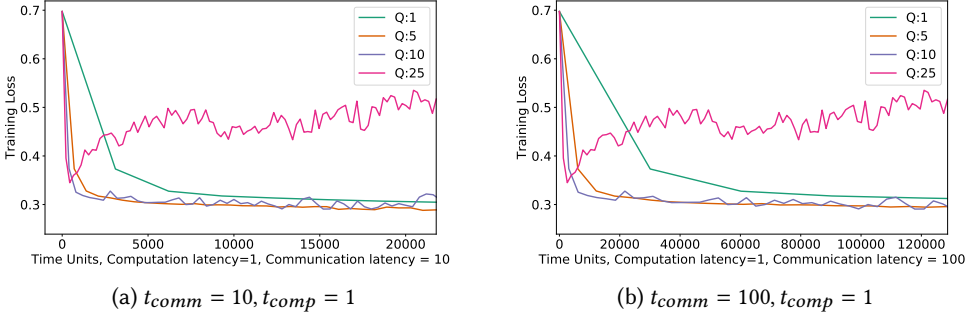


Fig. 6. LSTM on MIMIC III, training loss vs time units for variations of t_{comm} . $N=4, K=10$.

Theorem 1. It is to be noted that varying N introduces other forms of dissimilarity in this experiment as the neural network architectures are different due to the different dimensions of the input features for each silo for different values of N . However, the convergence rates for moderate values of $N = 4$ or $N = 16$ are not arbitrarily different and can be influenced with an appropriate learning rate. The $N = 1$ configuration, where all the features are in a single silo, outperforms other cases with multiple vertical partitions.

5.3.4 Latency vs convergence tradeoff. In the last set of experiments in Fig. 5 and Fig. 6, we now study the tradeoff between convergence rate and training latency of TDCD. In these experiments, we simulate a notion of training latency in our system model, where we denote the round trip communication latency between the hub and clients, and between hubs, as t_{comm} units. We denote the local computation latency of each step of training by $t_{comp} = 1$ unit. This will allow us to explore convergence properties of TDCD under different possible ratios of communication and computation latencies. Since for each communication round, i.e., Q local iterations, clients and hubs communicate twice and hubs communicate with each other once, the total latency of one communication round can be simplified as: $t_Q = 3 \times t_{comm} + Q \times t_{comp}$.

The results are shown Fig. 5 and Fig. 6. We again vary the number of local iterations Q and show the convergence of the global model. However, instead of plotting training iterations on the X-axis, we change the X-axis to *time units* or t_Q , via the notion of simulated communication latency t_{comm} and simulated compute latency t_{comp} . The Y-axis denotes training latency. We assume the compute latency per local training iteration in a client is $t_{comp} = 1$ unit of time. Since in communication

networks, the communication latency between nodes dominates the computation latency inside a node, we study higher values of t_{comm} compared to t_{comp} . We study two cases with a low t_{comm} of 10 units, and a high comm latency of 100 units. In Fig. 5, we fix the number of vertical partitions to $N = 2$ and horizontal partitions to $K = 10$ and use $\eta = 0.002$. In Fig. 6, we fix the number of vertical partitions to $N = 4$ and horizontal partitions to $K = 10$ and use $\eta = 0.0005$.

We immediately observe that as we increase Q , the training latency decreases. The trend is in contrast to Fig. 2a and Fig. 2b where increasing Q slows the convergence rate. The reason is because the experiment in Section 5.3.1 only considers training iterations. It does not consider the latency of each iteration. In Fig. 2a and Fig. 2b, we show training loss as a function of simulated latency. Hence, with increased Q , we are effectively allowing the system to train for more number of local iterations for a fixed communication latency. Further, in both the datasets, we observe that with increasing t_{comm} , the gap between the curves for different values of Q widens. This is because, in such scenarios, t_{comm} becomes the bottleneck; t_{comp} pays a negligible role in the overall latency. This implies that by judiciously selecting a value of $Q > 1$ local iterations at clients, TDCD can achieve faster convergence with respect to the training latency.

Overall, we observe that TDCD performs well and taking local steps even with vertically separated data has large benefits when communication latency is significant.

6 CONCLUSION

We have introduced TDCD, a communication efficient decentralized algorithm for a multi-tier network model with both horizontally and vertically partitioned data. We have provided theoretical analysis of the algorithm convergence and its dependence on the number of vertical partitions, the number of clients in each hub, and the number of local iterations. Finally, we have presented experimental results that validates our theory in practice. In future work, we plan to explore the possibility of hubs communicating with each other asynchronously to share information.

A PROOF OF THE THEOREM AND SUPPORTING LEMMAS

In this section provide the proofs of our theorem for convergence and the associated helping lemmas.

To facilitate the analysis, we first define an auxiliary local vector that represents the local view of the global model at each client. Let $\mathbf{y}_{k,j}^t$ denote the auxiliary weight vector used by client k in hub j to calculate the partial derivative $g_{k,j}$,

$$\mathbf{y}_{k,j}^t = [(\boldsymbol{\theta}_{-j}^{t_0})^\top, (\boldsymbol{\theta}_{k,j}^t)^\top]^\top \quad (15)$$

where, $\boldsymbol{\theta}_{-j}^{t_0}$ denotes the vector of all coordinates of $\tilde{\boldsymbol{\theta}}$ excluding block j at iteration $t_0 \leq t$, is the most recent iteration when the client k last updated the value of $\boldsymbol{\theta}_{-j}^{t_0}$ from its hub. $(\cdot)^\top$ represents transpose operation. The partial derivative $g_{k,j}$ at iteration t is a function of $\mathbf{y}_{k,j}^t$ and the minibatch selected at t_0 . With slight abuse of notation, we let:

$$g_{k,j}(\mathbf{y}_{k,j}^t) \stackrel{\text{def}}{=} g_{k,j}(\Phi_{-k,j}^{\zeta^{t_0}}, \Phi_{k,j}^{\zeta^{t_0}}, \zeta^{t_0})$$

We now define a vector whose individual elements are the average partial derivatives with respect to the entire dataset parameterized by the local weight vectors $\mathbf{y}_{k,j}$:

$$\mathbf{H}_{(j)}^t = \frac{1}{K_j} \sum_{k=1}^{K_j} \nabla_{(j)} \mathcal{L}(\mathbf{y}_{k,j}^t) \quad (16)$$

$$\mathbf{H}^t = [(\mathbf{H}_{(1)}^t)^T, \dots, (\mathbf{H}_{(N)}^t)^T]^T \quad (17)$$

Further, if Assumption 3 holds, then we have as a consequence

$$\mathbb{E}_{\zeta^{t_0}} \left[g_{k,j}(\mathbf{y}_{k,j}^t) \mid \{\mathbf{y}_{k,j}^r\}_{r=0}^{t_0} \right] = \nabla_{(j)} \mathcal{L}(\mathbf{y}_{k,j}^t) \quad (18)$$

$$\mathbb{E}_{\zeta^{t_0}} \left[\left\| g_{k,j}(\mathbf{y}_{k,j}^t) - \nabla_{(j)} \mathcal{L}(\mathbf{y}_{k,j}^t) \right\|^2 \mid \{\mathbf{y}_{k,j}^r\}_{r=0}^{t_0} \right] \leq \sigma_j^2. \quad (19)$$

where, the expectation is over the minibatch selected at iteration t_0 , conditioned on the algorithm iterates $\mathbf{y}_{k,j}^r$ up until t_0 . We recall the definition of the local stochastic partial derivative $g_{k,j}^t$ from (4). $g_{k,j}^t$ at iteration t is a function of $\mathbf{y}_{k,j}^t$ and the minibatch selected at t_0 . Our analysis looks at the evolution of the $\mathbf{y}_{k,j}^t$, $t_0 \leq t \leq t_0 + Q$, i.e. the interval between the latest communication round t_0 and the next communication round $t_0 + Q$.

For simplicity, we define $\mathbf{Y}^{t_0} \stackrel{\text{def}}{=} \{\mathbf{y}_{k,j}^r\}_{r=0}^{t_0}$ and ease the notation of the conditional expectation as the following:

$$\mathbb{E}_{\zeta^{t_0}} \left[\cdot \mid \{\mathbf{y}_{k,j}^r\}_{r=0}^{t_0} \right] \stackrel{\text{def}}{=} \mathbb{E}_{\zeta^{t_0}} \left[\cdot \mid \mathbf{Y}^{t_0} \right]$$

Here, by Assumption 3, we have $\mathbb{E}_{\zeta^{t_0}} \left[\mathbf{G}_{(j)}^t \mid \mathbf{Y}^{t_0} \right] = \mathbf{H}_{(j)}^t$.

A.1 PROOF OF SUPPORTING LEMMAS

We recall that we can write the evolution of the global model as:

$$\tilde{\boldsymbol{\theta}}^{t+1} = \tilde{\boldsymbol{\theta}}^t - \eta \mathbf{G}^t. \quad (20)$$

Here, we study the evolution of $\tilde{\boldsymbol{\theta}}$ at each iteration. We note that, the components of $\tilde{\boldsymbol{\theta}}_j$ are only realized every Q iterations at hub j when the hub communicates with its clients and with other hubs.

We make use of the following lemmas to simplify our analysis.

LEMMA 2.

$$\mathbb{E}_{\zeta^{t_0}} \left[\left\| \mathbf{G}_{(j)}^t - \mathbf{H}_{(j)}^t \right\|^2 \mid \mathbf{Y}^{t_0} \right] \leq \frac{\sigma_j^2}{K_j} \quad (21)$$

PROOF.

$$\begin{aligned} & \mathbb{E}_{\zeta^{t_0}} \left[\left\| \mathbf{G}_{(j)}^t - \mathbf{H}_{(j)}^t \right\|^2 \mid \mathbf{Y}^{t_0} \right] \\ &= \mathbb{E}_{\zeta^{t_0}} \left[\left\| \frac{1}{K_j} \sum_{k=1}^{K_j} g_{k,j}(\mathbf{y}_{k,j}^t) - \frac{1}{K_j} \sum_{k=1}^{K_j} \nabla_{(j)} \mathcal{L}(\mathbf{y}_{k,j}^t) \right\|^2 \mid \mathbf{Y}^{t_0} \right] \\ &= \frac{1}{K_j^2} \mathbb{E}_{\zeta^{t_0}} \left[\sum_{k=1}^{K_j} \left\| g_{k,j}(\mathbf{y}_{k,j}^t) - \nabla_{(j)} \mathcal{L}(\mathbf{y}_{k,j}^t) \right\|^2 \right. \\ & \quad \left. + \sum_{k=1}^{K_j} \sum_{l=1, l \neq k}^{K_j} \langle g_{k,j}(\mathbf{y}_{k,j}^t) - \nabla_{(j)} \mathcal{L}(\mathbf{y}_{k,j}^t), g_{l,j}(\mathbf{y}_{l,j}^t) - \nabla_{(j)} \mathcal{L}(\mathbf{y}_{l,j}^t) \rangle \mid \mathbf{Y}^{t_0} \right] \\ &= \frac{1}{K_j^2} \sum_{k=1}^{K_j} \mathbb{E}_{\zeta^{t_0}} \left[\left\| g_{k,j}(\mathbf{y}_{k,j}^t) - \nabla_{(j)} \mathcal{L}(\mathbf{y}_{k,j}^t) \right\|^2 \mid \mathbf{Y}^{t_0} \right] \end{aligned}$$

$$+ \frac{1}{K_j^2} \sum_{k=1}^{K_j} \sum_{l=1, l \neq k}^{K_j} \left\langle \mathbb{E}_{\zeta^{t_0}} \left[g_{k,j}(\mathbf{y}_{k,j}^t) - \nabla_{(j)} \mathcal{L}(\mathbf{y}_{k,j}^t) \middle| \mathbf{Y}^{t_0} \right], \mathbb{E}_{\zeta^{t_0}} \left[g_{l,j}(\mathbf{y}_{l,j}^t) - \nabla_{(j)} \mathcal{L}(\mathbf{y}_{l,j}^t) \middle| \mathbf{Y}^{t_0} \right] \right\rangle \quad (22)$$

Applying (8) in Assumption 3 to (22), we observe that we can bound the variance in the first sum and that the cross terms in the double summation evaluate to zero. We therefore have the following:

$$\begin{aligned} \mathbb{E}_{\zeta^{t_0}} \left[\left\| \mathbf{G}_{(j)}^t - \mathbf{H}_{(j)}^t \right\|^2 \middle| \mathbf{Y}^{t_0} \right] &\leq \frac{1}{K_j^2} \sum_{k=1}^{K_j} \sigma_j^2 \\ &\leq \frac{\sigma_j^2}{K_j} \end{aligned} \quad (23)$$

□

LEMMA 3.

$$\mathbb{E}_{\zeta^{t_0}} \left[\left\| \mathbf{G}^t \right\|^2 \middle| \mathbf{Y}^{t_0} \right] \leq \sum_{j=1}^N \frac{\sigma_j^2}{K_j} + \sum_{j=1}^N \frac{1}{K_j} \sum_{k=1}^{K_j} \left\| \nabla_{(j)} \mathcal{L}(\mathbf{y}_{k,j}^t) \right\|^2 \quad (24)$$

PROOF.

$$\begin{aligned} \mathbb{E}_{\zeta^{t_0}} \left[\left\| \mathbf{G}^t \right\|^2 \middle| \mathbf{Y}^{t_0} \right] &= \sum_{j=1}^N \mathbb{E}_{\zeta^{t_0}} \left[\left\| \mathbf{G}_{(j)}^t \right\|^2 \middle| \mathbf{Y}^{t_0} \right] \\ &\stackrel{(a)}{=} \sum_{j=1}^N \mathbb{E}_{\zeta^{t_0}} \left[\left\| \mathbf{G}_{(j)}^t - \mathbb{E}_{\zeta^{t_0}} \left[\mathbf{G}_{(j)}^t \middle| \mathbf{Y}^{t_0} \right] \right\|^2 \middle| \mathbf{Y}^{t_0} \right] + \sum_{j=1}^N \left\| \mathbb{E}_{\zeta^{t_0}} \left[\mathbf{G}_{(j)}^t \middle| \mathbf{Y}^{t_0} \right] \right\|^2 \\ &= \sum_{j=1}^N \mathbb{E}_{\zeta^{t_0}} \left[\left\| \mathbf{G}_{(j)}^t - \mathbf{H}_{(j)}^t \right\|^2 \middle| \mathbf{Y}^{t_0} \right] + \sum_{j=1}^N \left\| \mathbf{H}_{(j)}^t \right\|^2 \\ &\stackrel{(b)}{\leq} \sum_{j=1}^N \frac{\sigma_j^2}{K_j} + \sum_{j=1}^N \left\| \frac{1}{K_j} \sum_{k=1}^{K_j} \nabla_{(j)} \mathcal{L}(\mathbf{y}_{k,j}^t) \right\|^2 \\ &\stackrel{(c)}{\leq} \sum_{j=1}^N \frac{\sigma_j^2}{K_j} + \sum_{j=1}^N \frac{1}{K_j} \sum_{k=1}^{K_j} \left\| \nabla_{(j)} \mathcal{L}(\mathbf{y}_{k,j}^t) \right\|^2 \end{aligned} \quad (25)$$

where (a) follows directly from Assumption 3 and the definitions of \mathbf{G}^t and \mathbf{H}^t . The simplification in (b) is from Lemma 2, and (c) is because $\left\| \sum_{i=1}^N a_i \right\|^2 \leq N \sum_{i=1}^N \|a_i\|^2$. □

LEMMA 4.

$$\begin{aligned} \mathbb{E}_{\zeta^{t_0}} \left[\langle \nabla \mathcal{L}(\tilde{\boldsymbol{\theta}}^t), \mathbf{G}^t \rangle \middle| \mathbf{Y}^{t_0} \right] &= \frac{1}{2} \left\| \nabla \mathcal{L}(\tilde{\boldsymbol{\theta}}^t) \right\|^2 + \sum_{j=1}^N \frac{1}{2K_j} \sum_{k=1}^{K_j} \left\| \nabla_{(j)} \mathcal{L}(\mathbf{y}_{k,j}^t) \right\|^2 \\ &\quad - \sum_{j=1}^N \frac{1}{2K_j} \sum_{k=1}^{K_j} \left\| \nabla_{(j)} \mathcal{L}(\tilde{\boldsymbol{\theta}}^t) - \nabla_{(j)} \mathcal{L}(\mathbf{y}_{k,j}^t) \right\|^2 \end{aligned} \quad (26)$$

PROOF. We have:

$$\mathbb{E}_{\zeta^{t_0}} \left[\langle \nabla \mathcal{L}(\tilde{\boldsymbol{\theta}}^t), \mathbf{G}^t \rangle \middle| \mathbf{Y}^{t_0} \right] = \sum_{j=1}^N \left\langle \nabla_{(j)} \mathcal{L}(\tilde{\boldsymbol{\theta}}^t), \mathbb{E}_{\zeta^{t_0}} \left[\mathbf{G}_{(j)}^t \middle| \mathbf{Y}^{t_0} \right] \right\rangle$$

$$\begin{aligned}
& \stackrel{(a)}{=} \sum_{j=1}^N \left\langle \nabla_{(j)} \mathcal{L}(\tilde{\theta}^t), \mathbf{H}_{(j)}^t \right\rangle \\
& = \sum_{j=1}^N \frac{1}{K_j} \sum_{k=1}^{K_j} \langle \nabla_{(j)} \mathcal{L}(\tilde{\theta}^t), \nabla_{(j)} \mathcal{L}(\mathbf{y}_{k,j}^t) \rangle \\
& = \sum_{j=1}^N \frac{1}{2K_j} \sum_{k=1}^{K_j} \left[\left\| \nabla_{(j)} \mathcal{L}(\tilde{\theta}^t) \right\|^2 + \left\| \nabla_{(j)} \mathcal{L}(\mathbf{y}_{k,j}^t) \right\|^2 - \left\| \nabla_{(j)} \mathcal{L}(\tilde{\theta}^t) - \nabla_{(j)} \mathcal{L}(\mathbf{y}_{k,j}^t) \right\|^2 \right] \\
& = \frac{1}{2} \left\| \nabla \mathcal{L}(\tilde{\theta}^t) \right\|^2 + \sum_{j=1}^N \frac{1}{2K_j} \sum_{k=1}^{K_j} \left\| \nabla_{(j)} \mathcal{L}(\mathbf{y}_{k,j}^t) \right\|^2 \\
& \quad - \sum_{j=1}^N \frac{1}{2K_j} \sum_{k=1}^{K_j} \left\| \nabla_{(j)} \mathcal{L}(\tilde{\theta}^t) - \nabla_{(j)} \mathcal{L}(\mathbf{y}_{k,j}^t) \right\|^2
\end{aligned} \tag{27}$$

where, in (a), we use Assumption 3. \square

We now define a lemma to relate the expected local and expected global gradient.

LEMMA 5.

$$\mathbb{E} \left\| g_{k,j}(\mathbf{y}_{k,j}^t) \right\|^2 \leq \sigma_j^2 + \mathbb{E} \left\| \nabla_{(j)} \mathcal{L}(\mathbf{y}_{k,j}^t) \right\|^2 \tag{28}$$

where \mathbb{E} is the total expectation.

PROOF. We observe that at iteration t , where the latest communication between clients and hubs took place at iteration $t_0 \leq t$:

$$\begin{aligned}
\sigma_j^2 & \geq \mathbb{E} \left\| g_{k,j}(\mathbf{y}_{k,j}^t) - \nabla_{(j)} \mathcal{L}(\mathbf{y}_{k,j}^t) \right\|^2 \\
& = \mathbb{E} \left[\mathbb{E}_{\zeta^{t_0}} \left[\left\| g_{k,j}(\mathbf{y}_{k,j}^t) - \nabla_{(j)} \mathcal{L}(\mathbf{y}_{k,j}^t) \right\|^2 \middle| \mathbf{Y}^{t_0} \right] \right] \\
& = \mathbb{E} \left[\mathbb{E}_{\zeta^{t_0}} \left[\left\| g_{k,j}(\mathbf{y}_{k,j}^t) - \mathbb{E}_{\zeta^{t_0}} \left[g_{k,j}(\mathbf{y}_{k,j}^t) \middle| \mathbf{Y}^{t_0} \right] \right\|^2 \middle| \mathbf{Y}^{t_0} \right] \right] \\
& = \mathbb{E} \left[\mathbb{E}_{\zeta^{t_0}} \left[\left\| g_{k,j}(\mathbf{y}_{k,j}^t) \right\|^2 - \left\| \mathbb{E}_{\zeta^{t_0}} \left[g_{k,j}(\mathbf{y}_{k,j}^t) \middle| \mathbf{Y}^{t_0} \right] \right\|^2 \middle| \mathbf{Y}^{t_0} \right] \right] \\
& \stackrel{(a)}{=} \mathbb{E} \left[\mathbb{E}_{\zeta^{t_0}} \left\| g_{k,j}(\mathbf{y}_{k,j}^t) \right\|^2 \middle| \mathbf{Y}^{t_0} \right] - \mathbb{E} \left[\left\| \mathbb{E}_{\zeta^{t_0}} [g_{k,j}(\mathbf{y}_{k,j}^t) \middle| \mathbf{Y}^{t_0}] \right\|^2 \right] \\
& = \mathbb{E} \left\| g_{k,j}(\mathbf{y}_{k,j}^t) \right\|^2 - \mathbb{E} \left\| \nabla_{(j)} \mathcal{L}(\mathbf{y}_{k,j}^t) \right\|^2
\end{aligned} \tag{29}$$

Here the equality in (a) follows from (8) in Assumption 3. We can obtain Lemma 5 by rearranging (29). \square

A.2 PROOF OF THE THEOREM 1

PROOF. We now prove our main result. We return to the expression in (20), on which we use the Lipschitz condition and take expectation to obtain the following:

$$\begin{aligned}
& \mathbb{E}_{\zeta^{t_0}} \left[\mathcal{L}(\tilde{\theta}^{t+1}) \middle| \mathbf{Y}^{t_0} \right] - \mathcal{L}(\tilde{\theta}^t) \\
& \leq \mathbb{E}_{\zeta^{t_0}} \left[\langle \nabla \mathcal{L}(\tilde{\theta}^t), \tilde{\theta}^{t+1} - \tilde{\theta}^t \rangle \middle| \mathbf{Y}^{t_0} \right] + \frac{L}{2} \mathbb{E}_{\zeta^{t_0}} \left[\left\| \tilde{\theta}^{t+1} - \tilde{\theta}^t \right\|^2 \middle| \mathbf{Y}^{t_0} \right] \\
& \leq -\eta \mathbb{E}_{\zeta^{t_0}} \left[\langle \nabla \mathcal{L}(\tilde{\theta}^t), \mathbf{G}^t \rangle \middle| \mathbf{Y}^{t_0} \right] + \frac{\eta^2 L}{2} \mathbb{E}_{\zeta^{t_0}} \left[\left\| \mathbf{G}^t \right\|^2 \middle| \mathbf{Y}^{t_0} \right].
\end{aligned}$$

From Lemmas 3 and 4, we now have

$$\begin{aligned}
& \mathbb{E}_{\zeta^{t_0}} \left[\mathcal{L}(\tilde{\theta}^{t+1}) \middle| \mathbf{Y}^{t_0} \right] - \mathcal{L}(\tilde{\theta}^t) \\
& \leq -\frac{\eta}{2} \left\| \nabla \mathcal{L}(\tilde{\theta}^t) \right\|^2 - \sum_{j=1}^N \frac{\eta}{2K_j} \sum_{k=1}^{K_j} \left\| \nabla_{(j)} \mathcal{L}(\mathbf{y}_{k,j}^t) \right\|^2 + \sum_{j=1}^N \frac{\eta}{2K_j} \sum_{k=1}^{K_j} \left\| \nabla_{(j)} \mathcal{L}(\tilde{\theta}^t) - \nabla_{(j)} \mathcal{L}(\mathbf{y}_{k,j}^t) \right\|^2 \\
& \quad + \eta^2 L \sum_{j=1}^N \frac{1}{2K_j} \sum_{k=1}^{K_j} \left\| \nabla_{(j)} \mathcal{L}(\mathbf{y}_{k,j}^t) \right\|^2 + \eta^2 L \sum_{j=1}^N \frac{\sigma_j^2}{2K_j} \\
& \stackrel{(a)}{\leq} -\frac{\eta}{2} \left\| \nabla \mathcal{L}(\tilde{\theta}^t) \right\|^2 - \eta(1-\eta L) \sum_{j=1}^N \frac{1}{2K_j} \sum_{k=1}^{K_j} \left\| \nabla_{(j)} \mathcal{L}(\mathbf{y}_{k,j}^t) \right\|^2 \\
& \quad + \eta L_{\max}^2 \sum_{j=1}^N \frac{1}{2K_j} \sum_{k=1}^{K_j} \left\| \tilde{\theta}^t - \mathbf{y}_{k,j}^t \right\|^2 + \eta^2 L \sum_{j=1}^N \frac{\sigma_j^2}{2K_j}
\end{aligned} \tag{30}$$

where (a) follows from Assumption 1 and the definition of L_{\max} . Rearranging, we get

$$\begin{aligned}
\left\| \nabla \mathcal{L}(\tilde{\theta}^t) \right\|^2 & \leq \frac{2}{\eta} \left(\mathcal{L}(\tilde{\theta}^t) - \mathbb{E}_{\zeta^{t_0}} \left[\mathcal{L}(\tilde{\theta}^{t+1}) \middle| \mathbf{Y}^{t_0} \right] \right) + L_{\max}^2 \sum_{j=1}^N \frac{1}{K_j} \sum_{k=1}^{K_j} \left\| \tilde{\theta}^t - \mathbf{y}_{k,j}^t \right\|^2 + \eta L \sum_{j=1}^N \frac{\sigma_j^2}{K_j} \\
& \quad - (1-\eta L) \sum_{j=1}^N \frac{1}{K_j} \sum_{k=1}^{K_j} \left\| \nabla_{(j)} \mathcal{L}(\mathbf{y}_{k,j}^t) \right\|^2.
\end{aligned} \tag{31}$$

We now take the total expectation and average all iterates from $t = 0, \dots, T$

$$\begin{aligned}
\mathbb{E} \left[\frac{1}{T} \sum_{t=0}^{T-1} \left\| \nabla \mathcal{L}(\tilde{\theta}^t) \right\|^2 \right] & \leq \frac{2}{\eta T} \left(\mathcal{L}(\tilde{\theta}^0) - \mathcal{L}_{\inf} \right) + \frac{L_{\max}^2}{T} \sum_{t=0}^{T-1} \sum_{j=1}^N \frac{1}{K_j} \sum_{k=1}^{K_j} \mathbb{E} \left\| \tilde{\theta}^t - \mathbf{y}_{k,j}^t \right\|^2 + \eta L \sum_{j=1}^N \frac{\sigma_j^2}{K_j} \\
& \quad - \frac{1}{T} (1-\eta L) \sum_{t=0}^{T-1} \sum_{j=1}^N \frac{1}{K_j} \sum_{k=1}^{K_j} \mathbb{E} \left\| \nabla_{(j)} \mathcal{L}(\mathbf{y}_{k,j}^t) \right\|^2.
\end{aligned} \tag{32}$$

We now simplify the second and fourth terms in the above (32). Before proceeding further into the proof, we first state that for any vector θ we denote the values corresponding to the j th block of coordinates of θ by $\theta_{(j)}$.

We can simplify the second term in (32) as the follows:

$$\frac{1}{K_j} \sum_{k=1}^{K_j} \left\| \tilde{\theta}_{(j)}^t - \mathbf{y}_{k,j}^t \right\|^2 = \frac{1}{K_j} \sum_{k=1}^{K_j} \left\| \tilde{\theta}_j^t - \theta_{k,j}^t \right\|^2$$

$$\begin{aligned}
&= \frac{1}{K_j} \sum_{k=1}^{K_j} \left\| \boldsymbol{\theta}_{k,j}^t - \tilde{\boldsymbol{\theta}}_j^t - (\tilde{\boldsymbol{\theta}}_j^t - \tilde{\boldsymbol{\theta}}_j^{t_0}) \right\|^2 \\
&= \frac{1}{K_j} \left\| \left(\boldsymbol{\theta}_{k,j}^t - \tilde{\boldsymbol{\theta}}_j^{t_0} \right) - \left(\frac{1}{K_j} \sum_{l=1}^{K_j} (\boldsymbol{\theta}_{l,j}^t - \tilde{\boldsymbol{\theta}}_j^{t_0}) \right) \right\|^2.
\end{aligned} \tag{33}$$

We observe that, for an arbitrary set of vectors $\{\mathbf{z}_l\}_{l=1}^K$,

$$\begin{aligned}
\frac{1}{K} \sum_{k=1}^K \left\| \mathbf{z}_k - \frac{1}{K} \sum_{l=1}^K \mathbf{z}_l \right\|^2 &= \frac{1}{K} \sum_{k=1}^K \|\mathbf{z}_k\|^2 - \left\| \frac{1}{K} \sum_{k=1}^K \mathbf{z}_k \right\|^2 \\
&\leq \frac{1}{K} \sum_{k=1}^K \|\mathbf{z}_k\|^2.
\end{aligned} \tag{34}$$

Letting $\mathbf{z}_l = \boldsymbol{\theta}_{l,j}^t - \tilde{\boldsymbol{\theta}}_j^{t_0}$, we have

$$\begin{aligned}
\frac{1}{K_j} \sum_{k=1}^{K_j} \|\tilde{\boldsymbol{\theta}}_{(j)}^t - \mathbf{y}_{k,j,(j)}^t\|^2 &\leq \frac{1}{K_j} \sum_{k=1}^{K_j} \left\| \boldsymbol{\theta}_{k,j}^t - \tilde{\boldsymbol{\theta}}_j^{t_0} \right\|^2 \\
&\leq \frac{1}{K_j} \sum_{k=1}^{K_j} (t-1-t_0) \eta^2 \sum_{\tau=t_0}^{t-1} \|g_{k,j}(\mathbf{y}_{k,j}^\tau)\|^2 \\
&\leq \frac{Q\eta^2}{K_j} \sum_{k=1}^{K_j} \sum_{\tau=t_0}^{t-1} \|g_{k,j}(\mathbf{y}_{k,j}^\tau)\|^2.
\end{aligned} \tag{35}$$

Here, we can have (35), as $Q \geq t-1-t_0$ since we are considering the number of iterations between t_0 which is the latest communication between the hubs and clients, and the next communication round at iteration $t_0 + Q$.

Therefore the following holds:

$$\frac{1}{K_j} \sum_{k=1}^{K_j} \|\tilde{\boldsymbol{\theta}}_{(j)}^t - \mathbf{y}_{k,j,(j)}^t\|^2 \leq \frac{Q\eta^2}{K_j} \sum_{k=1}^{K_j} \sum_{\tau=t_0}^{t-1} \|g_{k,j}(\mathbf{y}_{k,j}^\tau)\|^2. \tag{36}$$

We now simplify the fourth term in (32) as the following:

$$\begin{aligned}
&L_{\max}^2 \sum_{j=1}^N \frac{1}{K_j} \sum_{k=1}^{K_j} \left\| \tilde{\boldsymbol{\theta}}^t - \mathbf{y}_{k,j}^t \right\|^2 \\
&\stackrel{(a)}{=} L_{\max}^2 \sum_{j=1}^N \frac{1}{K_j} \sum_{k=1}^{K_j} \left[\sum_{l \neq j}^N \left\| \tilde{\boldsymbol{\theta}}_{(l)}^t - \tilde{\boldsymbol{\theta}}_{(l)}^{t_0} \right\|^2 + \left\| \tilde{\boldsymbol{\theta}}_{(j)}^t - \mathbf{y}_{k,j,(j)}^t \right\|^2 \right] \\
&= L_{\max}^2 \sum_{j=1}^N \frac{1}{K_j} \sum_{k=1}^{K_j} \sum_{l \neq j}^N \left\| \tilde{\boldsymbol{\theta}}_{(l)}^{t_0} - \frac{\eta}{K_l} \sum_{\tau=t_0}^{t-1} \sum_{p=1}^{K_l} g_{p,l}(\mathbf{y}_{p,l}^\tau) - \tilde{\boldsymbol{\theta}}_{(l)}^{t_0} \right\|^2 + L_{\max}^2 \sum_{j=1}^N \frac{1}{K_j} \sum_{k=1}^{K_j} \left\| \tilde{\boldsymbol{\theta}}_{(j)}^t - \mathbf{y}_{k,j,(j)}^t \right\|^2 \\
&\stackrel{(b)}{\leq} L_{\max}^2 \sum_{j=1}^N \frac{1}{K_j} \sum_{k=1}^{K_j} \eta^2 (t-1-t_0) \sum_{l \neq j}^N \frac{1}{K_l} \sum_{\tau=t_0}^{t-1} \sum_{p=1}^{K_l} \|g_{p,l}(\mathbf{y}_{p,l}^\tau)\|^2 + L_{\max}^2 \sum_{j=1}^N \frac{1}{K_j} \sum_{k=1}^{K_j} \left\| \tilde{\boldsymbol{\theta}}_{(j)}^t - \mathbf{y}_{k,j,(j)}^t \right\|^2
\end{aligned}$$

$$\begin{aligned}
& \stackrel{(c)}{\leq} \eta^2 L_{\max}^2 Q \sum_{j=1}^N \frac{1}{K_j} \sum_{k=1}^{K_j} \sum_{l \neq j}^N \sum_{\tau=t_0}^{t-1} \frac{1}{K_l} \sum_{p=1}^{K_l} \left\| g_{p,l}(\mathbf{y}_{p,l}^\tau) \right\|^2 + L_{\max}^2 \sum_{j=1}^N \frac{1}{K_j} \sum_{k=1}^{K_j} \left\| \tilde{\boldsymbol{\theta}}_{(j)}^t - \mathbf{y}_{k,j,(j)}^t \right\|^2 \\
& = \eta^2 L_{\max}^2 Q(N-1) \sum_{j=1}^N \frac{1}{K_j} \sum_{\tau=t_0}^{t-1} \sum_{p=1}^{K_j} \left\| g_{p,j}(\mathbf{y}_{p,j}^\tau) \right\|^2 + L_{\max}^2 \sum_{j=1}^N \frac{1}{K_j} \sum_{k=1}^{K_j} \left\| \tilde{\boldsymbol{\theta}}_{(j)}^t - \mathbf{y}_{k,j,(j)}^t \right\|^2 \\
& \stackrel{(d)}{\leq} \eta^2 L_{\max}^2 Q(N-1) \sum_{j=1}^N \sum_{\tau=t_0}^{t-1} \sum_{p=1}^{K_j} \left\| g_{p,j}(\mathbf{y}_{p,j}^\tau) \right\|^2 + L_{\max}^2 \sum_{j=1}^N \frac{Q\eta^2}{K_j} \sum_{k=1}^{K_j} \sum_{\tau=t_0}^{t-1} \left\| g_{k,j}(\mathbf{y}_{k,j}^\tau) \right\|^2 \\
& = \eta^2 L_{\max}^2 QN \sum_{j=1}^N \sum_{\tau=t_0}^{t-1} \frac{1}{K_j} \sum_{p=1}^{K_j} \left\| g_{p,j}(\mathbf{y}_{p,j}^\tau) \right\|^2. \tag{37}
\end{aligned}$$

Here, in (a) we use the fact that each hub sent the updated model to its clients in iteration t_0 , where $t - t_0 \leq Q$. Hence the values in coordinate blocks l other than j of $\mathbf{y}_{k,j}^t$ are essentially $\tilde{\boldsymbol{\theta}}_l^{t_0}$, $l \neq j$, i.e. $\mathbf{y}_{k,j,(l)}^t = \tilde{\boldsymbol{\theta}}_{(l)}^{t_0}$, $l \neq j$. In (b), we use the inequality $\left\| \sum_{i=1}^N a_i \right\|^2 \leq N \sum_{i=1}^N \|a_i\|^2$ and in (c), we use the fact that $Q \geq t - 1 - t_0$. Finally, in (d) we use simplification from (36).

Therefore the following holds:

$$\begin{aligned}
& L_{\max}^2 \sum_{j=1}^N \frac{1}{K_j} \sum_{k=1}^{K_j} \left\| \tilde{\boldsymbol{\theta}}^t - \mathbf{y}_{k,j}^t \right\|^2 \\
& \leq \eta^2 L_{\max}^2 QN \left[\sum_{j=1}^N \sum_{\tau=t_0}^{t-1} \frac{1}{K_j} \sum_{p=1}^{K_j} \left\| g_{p,j}(\mathbf{y}_{p,j}^\tau) \right\|^2 \right]. \tag{38}
\end{aligned}$$

Applying (38), we can further bound (32) as

$$\begin{aligned}
\mathbb{E} \left[\frac{1}{T} \sum_{t=0}^{T-1} \left\| \nabla \mathcal{L}(\tilde{\boldsymbol{\theta}}^t) \right\|^2 \right] & \leq \frac{2}{\eta T} \left(\mathcal{L}(\tilde{\boldsymbol{\theta}}^0) - \mathcal{L}_{\inf} \right) + \frac{\eta^2 L_{\max}^2 QN}{T} \sum_{t=0}^{T-1} \sum_{j=1}^N \sum_{\tau=t_0}^{t-1} \frac{1}{K_j} \sum_{p=1}^{K_j} \mathbb{E} \left\| g_{p,j}(\mathbf{y}_{p,j}^\tau) \right\|^2 \\
& \quad + \eta L \sum_{j=1}^N \frac{\sigma_j^2}{K_j} - \frac{(1-\eta L)}{T} \sum_{t=0}^{T-1} \sum_{j=1}^N \frac{1}{K_j} \sum_{k=1}^{K_j} \mathbb{E} \left\| \nabla_{(j)} \mathcal{L}(\mathbf{y}_{k,j}^t) \right\|^2 \tag{39}
\end{aligned}$$

$$\begin{aligned}
& \stackrel{(a)}{\leq} \frac{2(\mathcal{L}(\tilde{\boldsymbol{\theta}}^0) - \mathcal{L}_{\inf})}{\eta T} + \frac{\eta^2 L_{\max}^2 Q^2 N}{T} \sum_{t=0}^{T-1} \sum_{j=1}^N \frac{1}{K_j} \sum_{p=1}^{K_j} \mathbb{E} \left\| g_{p,j}(\mathbf{y}_{p,j}^\tau) \right\|^2 \\
& \quad + \eta L \sum_{j=1}^N \frac{\sigma_j^2}{K_j} - \frac{(1-\eta L)}{T} \sum_{t=0}^{T-1} \sum_{j=1}^N \frac{1}{K_j} \sum_{k=1}^{K_j} \mathbb{E} \left\| \nabla_{(j)} \mathcal{L}(\mathbf{y}_{k,j}^t) \right\|^2 \tag{40}
\end{aligned}$$

$$\begin{aligned}
& \stackrel{(b)}{\leq} \frac{2(\mathcal{L}(\tilde{\boldsymbol{\theta}}^0) - \mathcal{L}_{\inf})}{\eta T} + \frac{\eta^2 L_{\max}^2 Q^2 N}{T} \sum_{t=0}^{T-1} \sum_{j=1}^N \frac{1}{K_j} \sum_{p=1}^{K_j} \left(\sigma_j^2 + \mathbb{E} \left\| \nabla_{(j)} \mathcal{L}(\mathbf{y}_{p,j}^t) \right\|^2 \right) \\
& \quad + \eta L \sum_{j=1}^N \frac{\sigma_j^2}{K_j} - \frac{(1-\eta L)}{T} \sum_{t=0}^{T-1} \sum_{j=1}^N \frac{1}{K_j} \sum_{k=1}^{K_j} \mathbb{E} \left\| \nabla_{(j)} \mathcal{L}(\mathbf{y}_{k,j}^t) \right\|^2 \tag{41} \\
& \leq \frac{2(\mathcal{L}(\tilde{\boldsymbol{\theta}}^0) - \mathcal{L}_{\inf})}{\eta T} + \eta L \sum_{j=1}^N \frac{\sigma_j^2}{K_j} + L_{\max}^2 \eta^2 \sum_{j=1}^N \sigma_j^2 Q^2 N
\end{aligned}$$

$$- \frac{1 - \eta L - \eta^2 L_{\max}^2 Q^2 N}{T} \sum_{t=0}^{T-1} \sum_{j=1}^N \frac{1}{K_j} \sum_{k=1}^{K_j} \mathbb{E} \left\| \nabla_{(j)} \mathcal{L}(y_{k,j}^t) \right\|^2 \quad (42)$$

where we can simplify the double summation in (a) because $t - 1 - t_0 \leq Q$, and in (b), we apply Lemma 5.

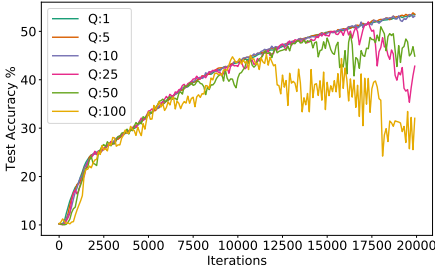
Assuming η is chosen so that $1 - \eta L - \eta^2 L_{\max}^2 Q^2 N \geq 0$, i.e., $0 \leq \eta \leq \min\left(\frac{1}{L}, \frac{1}{L_{\max} Q \sqrt{N}}\right)$, then we have

$$\mathbb{E} \left[\frac{1}{T} \sum_{t=0}^{T-1} \left\| \nabla \mathcal{L}(\tilde{\theta}^t) \right\|^2 \right] \leq \frac{2}{\eta T} \left(\mathcal{L}(\tilde{\theta}^0) - \mathcal{L}_{\inf} \right) + \eta L \sum_{j=1}^N \frac{\sigma_j^2}{K_j} + L_{\max}^2 \eta^2 Q^2 N \sum_{j=1}^N \sigma_j^2. \quad (43)$$

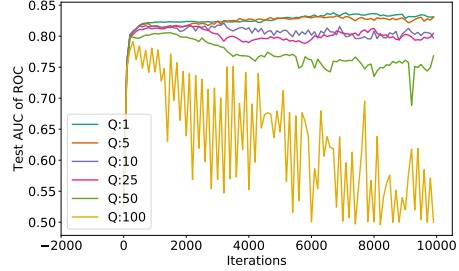
This completes the proof of Theorem 1. \square

B ADDITIONAL EXPERIMENTAL RESULTS

Here, we plot the test set accuracies for the Cifar 10 dataset and Area Under the Curve of the Receiver Operating Characteristics curve (AUC of ROC) for the MIMIC III dataset. It is to be noted that achieving better possible performance in unseen data (test set) can be optimized with hyperparameter tuning. However, our aim is to demonstrate that TDCD allows learning even with both horizontal and vertical partitioning of the data. We therefore do not attempt to perform early stopping in the experiments where we see overfitting on the test set and rather, provide the raw results. We see that in most of the cases in the following experiments, the results in the test set follow a similar pattern to what we described in Section 5.



(a) Variation with Q , Cifar 10, $N=2$, $K=10$



(b) Variation with Q , MIMIC III, $N=4$, $K=10$

Fig. 7. Performance of a CNN on Cifar10 dataset with test accuracy vs. iteration t , and LSTM on MIMIC III with AUC over ROC vs iteration t for variations of Q i.e., the number of local iterations.

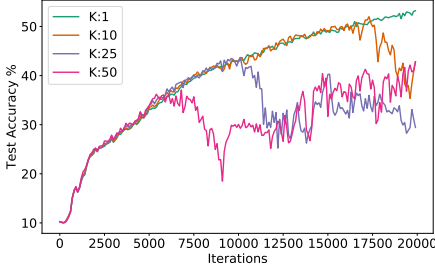
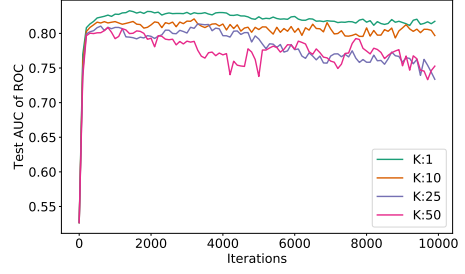
(a) Variation with K , Cifar 10, $N=2$, $Q=25$ (b) Variation with K , MIMIC III, $N=4$, $Q=10$

Fig. 8. Performance of a CNN on Cifar10 dataset with test accuracy vs. iteration t , and LSTM on MIMIC III with AUC over ROC vs iteration t for variations of K i.e., the number of horizontal partitions.

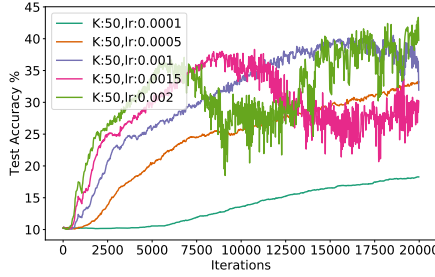
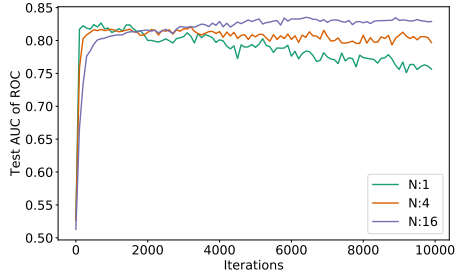
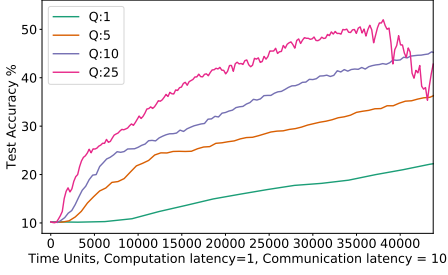
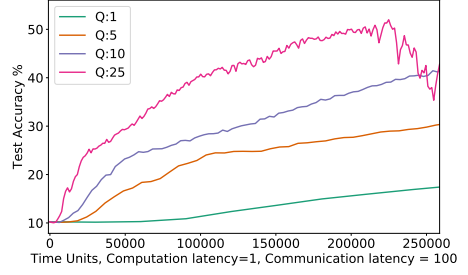
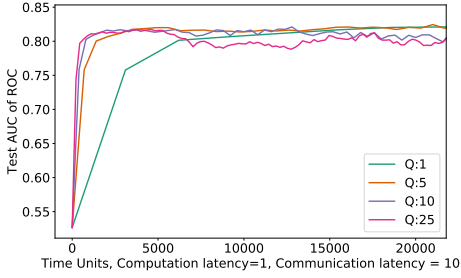
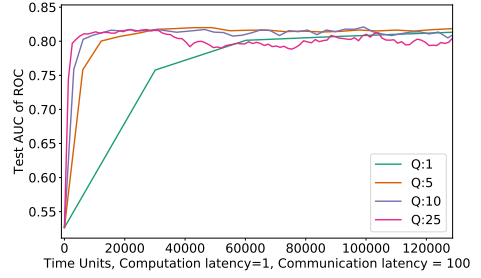
(a) Variation of η with high K , Cifar 10, $N=2$, $Q=25$ (b) Variation with N , MIMIC III, $K=10$, $Q=10$

Fig. 9. (a) Performance of a CNN on Cifar10 dataset with test accuracy vs. iteration t with effect of η on large values of K (b) LSTM on MIMIC III with AUC over ROC vs iteration t with effect of η on large values of K .

(a) $t_{comm} = 10, t_{comp} = 1$ (b) $t_{comm} = 100, t_{comp} = 1$ Fig. 10. CNN on Cifar 10, test accuracy vs time units for variations of t_{comm} . $N=2, K=10$.(a) $t_{comm} = 10, t_{comp} = 1$ (b) $t_{comm} = 100, t_{comp} = 1$ Fig. 11. LSTM on MIMIC III, AUC over ROC vs time units for variations of t_{comm} . $N=4, K=10$.

ACKNOWLEDGMENTS

This work is supported by the Rensselaer-IBM AI Research Collaboration (<http://airc.rpi.edu>), part of the IBM AI Horizons Network (<http://ibm.biz/AIHorizons>), and by the National Science Foundation under grants CNS 1553340 and CNS 1816307. A preliminary conference version of this work has been accepted in [4].

REFERENCES

- [1] Léon Bottou, Frank E Curtis, and Jorge Nocedal. 2018. Optimization methods for large-scale machine learning. *Siam Review* 60, 2 (2018), 223–311.
- [2] Timothy Castiglia, Anirban Das, and Stacy Patterson. 2021. Multi-Level Local SGD: Distributed SGD for Heterogeneous Hierarchical Networks. In *International Conference on Learning Representations*. OpenReview.net. <https://openreview.net/forum?id=C70cp4Cn32>
- [3] Tianyi Chen, Xiao Jin, Yuejiao Sun, and Wotao Yin. 2020. VAFL: a Method of Vertical Asynchronous Federated Learning. arXiv:cs.LG/2007.06081
- [4] A. Das and S. Patterson. 2021. Multi-Tier Federated Learning For Vertically Partitioned Data. In *ICASSP 2021 - 2021 IEEE International Conference on Acoustics, Speech and Signal Processing (ICASSP) (to appear)*.
- [5] Siwei Feng and Han Yu. 2020. Multi-Participant Multi-Class Vertical Federated Learning. arXiv:cs.LG/2001.11154
- [6] Farzin Haddadpour and Mehrdad Mahdavi. 2019. On the Convergence of Local Descent Methods in Federated Learning. arXiv:cs.LG/1910.14425
- [7] Stephen Hardy, Wilko Henecka, Hamish Ivey-Law, Richard Nock, Giorgio Patrini, Guillaume Smith, and Brian Thorne. 2017. Private federated learning on vertically partitioned data via entity resolution and additively homomorphic encryption. arXiv:cs.LG/1711.10677
- [8] Hrayr Harutyunyan, Hrant Khachatrian, David C. Kale, Greg Ver Steeg, and Aram Galstyan. 2019. Multitask learning and benchmarking with clinical time series data. *Scientific Data* 6, 1 (2019), 96. <https://doi.org/10.1038/s41597-019-0103-9>
- [9] Alistair EW Johnson, Tom J Pollard, Lu Shen, H Lehman Li-Wei, Mengling Feng, Mohammad Ghassemi, Benjamin Moody, Peter Szolovits, Leo Anthony Celi, and Roger G Mark. 2016. MIMIC-III, a freely accessible critical care database. *Scientific data* 3, 1 (2016), 1–9.
- [10] Peter Kairouz, H. Brendan McMahan, Brendan Avent, et al. 2021. Advances and Open Problems in Federated Learning. arXiv:cs.LG/1912.04977
- [11] Dongyeop Kang, Woosang Lim, Kijung Shin, Lee Sael, and U Kang. 2014. Data/Feature Distributed Stochastic Coordinate Descent for Logistic Regression. In *Proceedings of the 23rd ACM International Conference on Conference on Information and Knowledge Management, CIKM 2014, November 3-7, 2014*. ACM, Shanghai, China, 1269–1278. <https://doi.org/10.1145/2661829.2662082>
- [12] Ahmed Khaled, Konstantin Mishchenko, and Peter Richtárik. 2020. First Analysis of Local GD on Heterogeneous Data. arXiv:cs.LG/1909.04715
- [13] Jakub Konečný, H. Brendan McMahan, Daniel Ramage, and Peter Richtárik. 2016. Federated Optimization: Distributed Machine Learning for On-Device Intelligence. arXiv:cs.LG/1610.02527
- [14] Alex Krizhevsky, Geoffrey Hinton, et al. 2009. Learning multiple layers of features from tiny images.
- [15] Tian Li, Anit Kumar Sahu, Manzil Zaheer, Maziar Sanjabi, Ameet Talwalkar, and Virginia Smith. 2020. Federated Optimization in Heterogeneous Networks. In *Proceedings of Machine Learning and Systems*, Vol. 2. 429–450. <https://proceedings.mlsys.org/paper/2020/file/38af86134b65d0f10fe33d30dd76442e-Paper.pdf>
- [16] Yang Liu, Yan Kang, Xinwei Zhang, Liping Li, Yong Cheng, Tianjian Chen, Mingyi Hong, and Qiang Yang. 2020. A Communication Efficient Collaborative Learning Framework for Distributed Features. arXiv:cs.LG/1912.11187 Presented in Workshop on Federated Learning for Data Privacy and Confidentiality, NeurIPS 2019.
- [17] Dhruv Mahajan, S. Sathya Keerthi, and S. Sundararajan. 2017. A distributed block coordinate descent method for training l1 regularized linear classifiers. *Journal of Machine Learning Research* 18, 91 (2017), 1–35. <http://jmlr.org/papers/v18/14-484.html>
- [18] H. Brendan McMahan, Eider Moore, Daniel Ramage, Seth Hampson, and Blaise Agüera y Arcas. 2017. Communication-Efficient Learning of Deep Networks from Decentralized Data. arXiv:cs.LG/1602.05629
- [19] Peter Richtárik and Martin Takáč. 2016. Distributed coordinate descent method for learning with big data. *The Journal of Machine Learning Research* 17, 1 (2016), 2657–2681.
- [20] Sebastian U. Stich. 2019. Local SGD Converges Fast and Communicates Little. In *International Conference on Learning Representations*. OpenReview.net. <https://openreview.net/forum?id=S1g2JnRcFX>
- [21] Chang Sun, Lianne Ippel, Johan Van Soest, Birgit Wouters, Alexander Malic, Onaopepo Adekunle, Bob van den Berg, Ole Musmann, Annemarie Koster, Carla van der Kallen, et al. 2019. A Privacy-Preserving Infrastructure for Analyzing

- Personal Health Data in a Vertically Partitioned Scenario. *Studies in health technology and informatics* 264 (2019), 373–377.
- [22] Paul Tseng and Sangwoon Yun. 2009. A coordinate gradient descent method for nonsmooth separable minimization. *Mathematical Programming* 117, 1-2 (2009), 387–423.
 - [23] Jianyu Wang and Gauri Joshi. 2019. Cooperative SGD: A unified Framework for the Design and Analysis of Communication-Efficient SGD Algorithms. arXiv:[cs.LG/1808.07576](https://arxiv.org/abs/cs.LG/1808.07576)
 - [24] Jianyu Wang, Anit Kumar Sahu, Zhouyi Yang, Gauri Joshi, and Soummya Kar. 2019. MATCHA: Speeding Up Decentralized SGD via Matching Decomposition Sampling. In *2019 Sixth Indian Control Conference (ICC)*. IEEE, Hyderabad, India, 299–300. <https://doi.org/10.1109/ICC47138.2019.9123209>
 - [25] Jiayi Wang, Shiqiang Wang, Rong-Rong Chen, and Mingyue Ji. 2020. Local Averaging Helps: Hierarchical Federated Learning and Convergence Analysis. *arXiv preprint arXiv:2010.12998* (2020).
 - [26] Shiqiang Wang, Tiffany Tuor, Theodoros Salonidis, Kin K Leung, Christian Makaya, Ting He, and Kevin Chan. 2019. Adaptive federated learning in resource constrained edge computing systems. *IEEE Journal on Selected Areas in Communications* 37, 6 (2019), 1205–1221.
 - [27] Qiang Yang, Yang Liu, Tianjian Chen, and Yongxin Tong. 2019. Federated Machine Learning: Concept and Applications. *ACM Transactions on Intelligent Systems and Technology* 10, 2, Article 12 (Jan. 2019), 19 pages.
 - [28] Shengwen Yang, Bing Ren, Xuhui Zhou, and Liping Liu. 2019. Parallel Distributed Logistic Regression for Vertical Federated Learning without Third-Party Coordinator. arXiv:[cs.LG/1911.09824](https://arxiv.org/abs/cs.LG/1911.09824)
 - [29] Hao Yu, Sen Yang, and Shenghuo Zhu. 2019. Parallel restarted SGD with faster convergence and less communication: Demystifying why model averaging works for deep learning. In *Proceedings of the AAAI Conference on Artificial Intelligence*, Vol. 33. AAAI Press, Honolulu, Hawaii, USA, 5693–5700.